Terahertz conductivity of doped silicon calculated using the ensemble Monte Carlo/finite-difference time-domain simulation technique

K. J. Willis,[a] S. C. Hagness,[b] and I. Knezevic[c]
Department of Electrical and Computer Engineering, University of Wisconsin–Madison, 1415 Engineering Drive, Madison, Wisconsin 53706-1691, USA

(Received 15 December 2009; accepted 13 January 2010; published online 9 February 2010)

We present terahertz-frequency characterization of doped silicon via a multiphysics numerical technique that couples ensemble Monte Carlo (EMC) simulation of carrier transport and a finite-difference time-domain (FDTD) solver of Maxwell's curl equations. We elucidate the importance of rigorous enforcement of Gauss's law, in order to avoid unphysical charge buildup and enhance solver accuracy. The calculated complex conductivity of doped bulk silicon shows excellent agreement with available experimental data. This comprehensive microscopic simulator is a valuable predictive tool in the terahertz frequency range, where experimental data are scarce and the Drude model inadequate. © *2010 American Institute of Physics*. [doi:10.1063/1.3308491]

At frequencies below 100 GHz, the electrical conductivity σ of doped silicon is weakly dependent on frequency and well represented by the Drude model,[1,2] which relates complex conductivity, $\sigma(\omega)=\sigma(0)/(1-i\omega\tau)$, to the semiconductor's dc conductivity, $\sigma(0)=ne^2\tau/m$, where n is the carrier density, τ is the momentum relaxation time, and m is the carrier effective mass. As ω approaches terahertz (THz) frequencies, $\omega\tau\approx 1$, and σ becomes complex and strongly frequency-dependent. In this regime the Drude model is no longer adequate.[3] Several empirical fits have been proposed,[2–5] but, because of the scarcity of experimental data,[2,6] none is sufficiently parameterized to be broadly adopted. Therefore, a comprehensive simulation of THz-frequency conduction in doped semiconductors that is based on a detailed microscopic picture of carrier-field interaction promises to fill an important gap in our understanding of high-frequency transport.

In this letter, we characterize doped bulk silicon under THz-frequency excitation via a multiphysics numerical technique that combines the ensemble Monte Carlo (EMC) and finite-difference time-domain (FDTD) methods. EMC is a numerical technique used to describe diffusive carrier transport through a stochastic solution of the Boltzmann transport equation.[7] FDTD is a full-wave numerical technique for solving the time-dependent Maxwell's curl equations.[8] In the combined EMC/FDTD technique, carrier motion in EMC produces current density that acts as a source for FDTD electromagnetic field calculations; in turn, the fields calculated by FDTD accelerate each carrier in EMC through the Lorentz force.[6,9] Here, we emphasize the paramount importance of the explicit enforcement of Gauss's law for the overall accuracy and speed of the EMC/FDTD simulation. First, we explicitly enforce the continuity equation in order to ensure that the fields calculated by FDTD satisfy Gauss's law. This enforcement also eliminates the need for repeated solution of Poisson's equation during runtime. Second, we identify problems involving spurious charge buildup caused by improperly initialized electrostatic fields or improper treatment of the electrostatics near the boundary of the simulation domain, and offer efficient solutions to both problems. These advances vastly enhance the accuracy of the EMC/FDTD technique, as demonstrated by the excellent agreement between the computed complex conductivity of doped silicon and experimental results from Ref. 3.

We define a two-dimensional (2D) computational domain in the xy-plane (Fig. 1), with the dielectric constant of silicon ($\epsilon_r=11.8$) assumed throughout. The coupled EMC/FDTD region is enclosed by the white rectangle in Fig. 1. In the region between the white solid and dashed black lines, the time evolution of the fields is governed solely by Maxwell's equations, solved via FDTD with no coupling to EMC. In both regions, we set σ to zero in the FDTD update equations. The region exterior to the dashed black line is treated by convolutional perfectly matched layer absorbing boundary conditions which attenuate outward-propagating

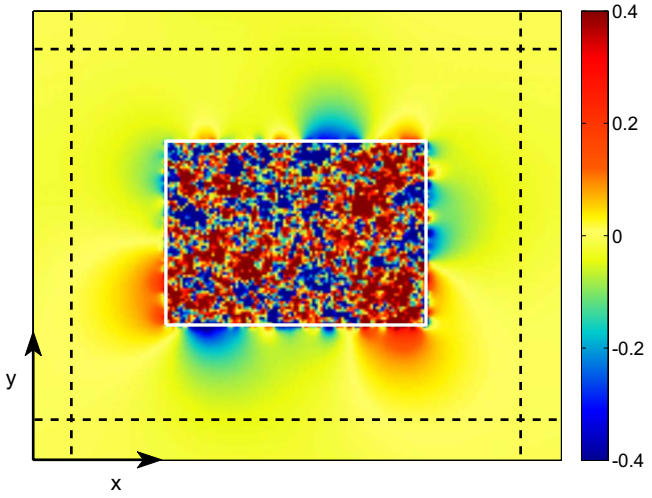

FIG. 1. (Color online) Snapshot of the 2D electrostatic potential Φ (color bar scale is in millivolts) throughout the computational domain in the absence of external excitation. The white box encloses the region in which EMC and FDTD simulations are coupled. Φ varies rapidly within the coupled region due to random placement of electrons and ions. The black dashed lines indicate the boundaries between the FDTD-domain on the inside and the convolutional perfectly matched-layer absorbing boundary conditions on the outside.

[a]Electronic mail: keelywillis@gmail.com.
[b]Electronic mail: hagness@engr.wisc.edu.
[c]Electronic mail: knezevic@engr.wisc.edu.

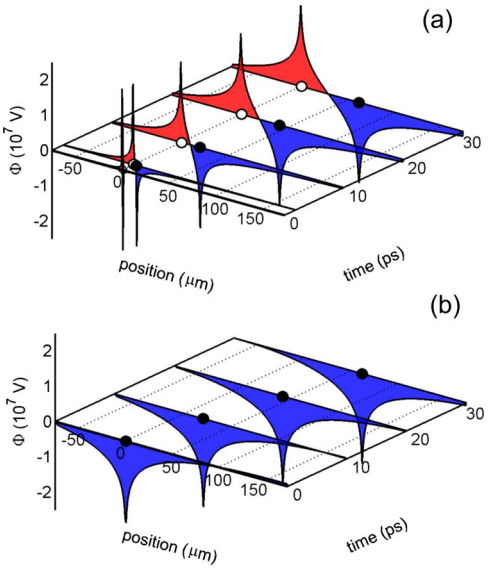

FIG. 2. (Color online) Electrostatic potential Φ due to the motion of a single electron, calculated from FDTD electric fields. (a) If the electrostatic field is initialized to zero, the electron's inception point appears to be charge neutral. As the electron moves, it leaves an artificial immobile hole behind. (b) When the electrostatic fields are initialized according to the solution to Poisson's equation for the electron's charge density, FDTD produces appropriate electrostatic fields for the pointlike moving particle.

electromagnetic waves by more than 80 dB.[8] Continuous THz-frequency plane waves are introduced via the analytic field propagation total-field/scattered-field formulation.[10] TE_z-polarized plane waves, comprising E_y and H_z components, impinge upon the coupled region from the left. The plane waves propagate along the x-direction, so the dominant force on the carriers is directed along y.

Gauss's law is implicitly satisfied by FDTD fields for EMC charges if the continuity equation,[8,11]

$$\nabla \cdot \vec{J} = -\frac{\partial \rho}{\partial t}, \tag{1}$$

is enforced where $\vec{J}$ is the current density and ρ is the charge density. In the typical quasielectrostatic EMC implementation which includes the numerical solution of Poisson's equation, ρ and $\vec{J}$ are spatially collocated on the grid and the continuity equation Eq. (1) is trivially satisfied. In contrast, in the EMC/FDTD simulation domain, $\vec{J}$ and ρ are assigned to two different, spatially staggered grids. The small approximations inherent to the grid assignment of $\vec{J}$ and ρ in the coupled EMC/FDTD region can result in a violation of Eq. (1). Here, we explicitly enforce Eq. (1) by calculating a carrier's contribution to $\vec{J}$ from its change in position over a time step rather than from its known instantaneous velocity. The resulting $\vec{J}$ is assigned to the grid according to the carrier's spatial charge profile.[11,12] An important advantage of the explicit enforcement of the continuity equation, and thereby the implicit satisfaction of Gauss's law, is that long-range Coulomb interactions among carriers are automatically accounted for during the simulation. This eliminates the need for repeated solution of Poisson's equation during runtime and dramatically increases computational speed.

Improper use of initialization schemes and boundary conditions in EMC/FDTD simulations can lead to spurious charge accumulation and violations of Gauss's law. In Fig. 2, we see the evolution of the electrostatic potential, Φ, for an EMC/FDTD simulation that involves a single electron moving with constant velocity in the 2D grid. Here, Φ is obtained through a line integration of FDTD electric fields from a reference grid point to a grid point of interest located along the electron's trajectory. FDTD electric fields are commonly initialized to zero, which corresponds to a charge-neutral domain. If this practice is adopted here, as the electron moves away from its point of origin, the electrostatic fields of an artificial hole are left behind [Fig. 2(a)]. If, however, the initial electric fields satisfy Gauss's law, the FDTD electromagnetic system will subsequently describe a moving electron, as expected [Fig. 2(b)]. We achieve proper initialization of the FDTD grid using electrostatic fields obtained by solving Poisson's equation for the initial charge distribution according tothe successive-over-relaxation method. Prior to the launch of the electromagnetic wave, the initial electric field satisfies Gauss's law, and the initial magnetic field is zero.

A second potential source of deviation from Gauss's law is spurious charge buildup at the boundary between the coupled EMC/FDTD region and the surrounding FDTD-only region (Fig. 1). EMC carriers reflect specularly from the left and the right boundary of the coupled region (their velocity normal to the boundary is inverted), in keeping with the expected zero net current through each of these boundaries. In contrast, as the dominant force acting on carriers and the current flow are in the y-direction, boundary conditions should allow unrestricted carrier motion and maintain the ensemble momentum in this direction. Therefore, carriers are subject to periodic boundary conditions at the top and bottom boundary of the EMC/FDTD coupled region: as a carrier exits one side of the region, it is injected at the opposite side with unaltered momentum. However, the instantaneous vanishing or emergence of carriers at the top and bottom boundaries of the coupled region is in conflict with Maxwell's equations. As a result, the electrostatic fields associated with that electron before its disappearance remain tethered to the boundary and act as a residual negative charge. Similarly, as the same electron is injected at the opposite boundary and moves into the coupled EMC/FDTD region, an effective hole's field is left behind, similar to what we saw in Fig. 2. Therefore, effective charge builds up on the top and bottom boundaries, impedes the flow of current along y and results in a lower calculated σ. To eliminate this source of error, every time an electron is removed (injected) at the coupled-region boundary, the electrostatic fields that accompany the electron (artificial hole) are also removed. To avoid repetitious runtime computations and maximize efficiency, in the solver initialization phase we solve Poisson's equation and calculate the electrostatic fields for a single electron (hole) located at different positions along the coupled-region boundary (250 distinct locations per boundary of an outer-layer grid cell, constituting a fine boundary grid). During runtime, we calculate the intercept between the electron trajectory and the boundary and force it onto the nearest location on the boundary grid; this position determines the appropriate precalculated electron (hole) electrostatic field, that is to be removed from the boundary at which the electron vanishes (emerges).

In order to determine the complex conductivity of doped silicon as a function of frequency, we calculate the electric-field and current-density phasors in the coupled EMC/FDTD region. Due to thermal electron motion, the EMC-computed

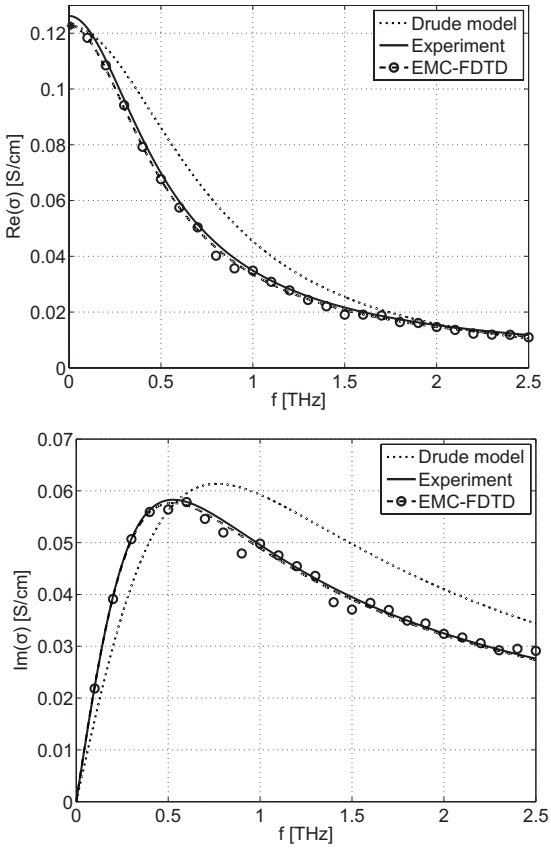

FIG. 3. Frequency-dependent conductivity, σ, of n-type silicon doped to 5.47×10^{14} cm^{-3}. Symbols represent the results of the EMC/FDTD numerical calculation, and the dashed line is an analytical best fit to the EMC/FDTD data, to guide the eye. The solid curve represents a faithful analytical fit to the experimental data of Ref. 3. Conductivity from the Drude model (dotted curve) is calculated using the known doping density and the corresponding electron mobility.

current density and the FDTD-computed fields are very noisy. We reduce the impact of this noise on conductivity calculations via spatial averaging of the extracted phasor quantities over small regions surrounding each grid location. The effective linear-regime conductivity is then computed as

$$\sigma(\omega) = \frac{\vec{E}(\omega)\cdot\vec{J}^{*}(\omega)}{|\vec{E}(\omega)|^{2}}, \tag{2}$$

where $\vec{E}(\omega)$ and $\vec{J}(\omega)$ are the electric-field and current-density phasors after the noise-reducing averaging procedure. In Fig. 3, we compare the calculated σ for n-type Si doped to 5.47×10^{14} cm^{-3} with experimental data obtained by Jeon and Grischkowsky via reflecting THz time-domain spectroscopy.[3] EMC/FDTD results show excellent agreement with experiment. The dramatic improvement in the agreement between the EMC/FDTD results and the experiment over those reported previously[6,13] results directly from the rigorous enforcement of Gauss's law, as described above. The Drude-model conductivity, calculated by using the doping density and the corresponding low-field mobility, differs significantly from both numerical and experimental data (Fig. 3). The disagreement is quite pronounced in the imaginary part of the conductivity, which describes an effective change in the dielectric constant.

In summary, we have presented the THz-regime conductivity calculation for lightly doped silicon using a combined EMC/FDTD simulation tool. We have elucidated the importance of strict enforcement of Gauss's law to avoid artificial charge buildup and dramatically increase the solver accuracy. As a result, the calculated conductivity data reproduce the experimental data to an outstanding degree. EMC/FDTD is an accurate and efficient simulation tool, holding promise as a highly predictive method for full characterization of semiconductors at THz frequencies.

This work has been supported by the AFOSR (Award No. FA9550-08-1-0052) and by the Wisconsin Alumni Research Foundation.

[1]R. T. Kinasewitz and B. Senitzky, J. Appl. Phys. **54**, 3394 (1983).
[2]M. van Exter and D. Grischkowsky, Phys. Rev. B **41**, 12140 (1990).
[3]T. I. Jeon and D. Grischkowsky, Phys. Rev. Lett. **78**, 1106 (1997).
[4]M. C. Beard, G. M. Turner, and C. A. Schmuttanmaer, Phys. Rev. B **62**, 15764 (2000).
[5]N. V. Smith, Phys. Rev. B **64**, 155106 (2001).
[6]K. J. Willis, S. C. Hagness, and I. Knezevic, J. Comput. Electron. **8**, 153 (2009).
[7]C. Jacoboni and L. Reggiani, Rev. Mod. Phys. **55**, 645 (1983).
[8]A. Taflove and S. C. Hagness, *Computational Electrodynamics: The Finite-Difference Time-Domain Method*, 3rd ed. (Artech House, Norwood, MA, 2005).
[9]R. O. Grondin, S. El-Ghazaly, and S. M. Goodnick, IEEE Trans. Microwave Theory Tech. **47**, 817 (1999).
[10]K. Abdijalilov and J. B. Schneider, IEEE Antennas Wireless Propag. Lett. **5**, 454 (2006).
[11]J. Villasenor and O. Buneman, Comput. Phys. Commun. **69**, 306 (1992).
[12]R. Barthelmé and C. Parzani, *Numerical Methods for Hyperbolic and Kinetic Problems* (European Mathematical Society, Marseille, France, 2005), pp. 7–28.
[13]K. J. Willis, S. C. Hagness, and I. Knezevic, "A Global EMC-FDTD Simulation Tool for High-Frequency Carrier Transport in Semiconductors," Proceedings of the 13th International Workshop on Computational Electronics (IWCE-13, 2009), pp. 265–268 (http://dx.doi.org/10.1109/IWCE.2009.5091080).